

1 **Mineralization of pentachlorophenol by**  
2 **ferrioxalate-assisted solar photo-Fenton process at**  
3 **mild pH**

4 Zhihong Ye<sup>a,b</sup>, Ignasi Sirés<sup>b</sup>, Hui Zhang<sup>a,\*</sup>, Yao-Hui Huang<sup>c,\*</sup>

5 *<sup>a</sup>Department of Environmental Science and Engineering, Wuhan University, Wuhan*  
6 *430079, China*

7 *<sup>b</sup>Laboratori d'Electroquímica dels Materials i del Medi Ambient, Departament de*  
8 *Química Física, Facultat de Química, Universitat de Barcelona, Martí i Franquès*  
9 *1-11, 08028 Barcelona, Spain*

10 *<sup>c</sup>Department of Chemical Engineering, National Cheng Kung University, Tainan 701,*  
11 *Taiwan*

12 \* Corresponding author: *E-mail address: eeng@whu.edu.cn. (H. Zhang)*

13 *E-mail address: yhhuang@mail.ncku.edu.tw (Y.-H. Huang)*

14

15 **Abstract**

16 This work reports the use of ferrioxalate complexes to assist solar photo-Fenton  
17 treatment of pentachlorophenol (PCP) in aqueous medium at mild pH, which inhibits  
18 the precipitation of iron hydroxides and allows working at a low iron dosage. The  
19 experimental parameters were optimized by assessing the effect of initial  
20 concentrations of H<sub>2</sub>O<sub>2</sub> (0-2.5 mM) and Fe(II) (2-10 mg/L), pH (3.0-9.0) and  
21 iron/oxalic acid molar ratios (1:0-1:13.5) on total organic carbon (TOC) removal.  
22 Ferrioxalate-assisted solar photo-Fenton achieved 97.5% mineralization in 120 min,  
23 clearly outperforming conventional Fenton and solar photo-Fenton. The presence of  
24 photosensitive ferrioxalate complexes accounted for the enhancement, as a result of  
25 Fe(II) regeneration that accelerated the hydroxyl radical (<sup>•</sup>OH) production. The time  
26 course of H<sub>2</sub>O<sub>2</sub> and Fe(II) concentrations was evaluated under different iron/oxalic  
27 acid ratios. The five carboxylic acids determined by ion-exclusion HPLC and the  
28 eight aromatic by-products identified by GC-MS allowed the proposal of a  
29 degradation pathway that included hydroxylation, dechlorination and dimerization  
30 steps. Complete chloride ion release was achieved after 90 min of treatment.

31 *Keywords:* Ferrioxalate complexes; Mild pH; Mineralization; Pentachlorophenol;

32 Solar photo-Fenton

33

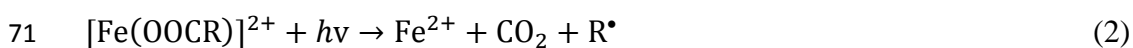
## 34 **1. Introduction**

35 Chlorophenols, listed as priority pollutants by most water directives worldwide  
36 due to their high toxicity, are still massively employed in industrial and agricultural  
37 activities (Hechmi et al., 2016; Khuzwayo and Chirwa, 2017). Pentachlorophenol  
38 (PCP,  $C_6HCl_5O$ ), the highest chlorinated phenol, is widely used as herbicide,  
39 fungicide, insecticide and disinfectant, showing main applications in agriculture,  
40 wood preservation and industry (Amendola et al., 2017; Tsoufis et al., 2017).  
41 Although large-scale manufacture and application of PCP have been banned in  
42 Taiwan and mainland China since 1984 and 1997, respectively, its presence in water  
43 and soil has been regularly reported in the last three decades (Shih et al., 2016). Due  
44 to its long-term persistence, high toxicity and carcinogenicity, wastewater  
45 contaminated with PCP must be conveniently treated before being discharged or  
46 reused (Cui et al., 2017).

47 The solubility of PCP, with  $pK_a = 4.75$  (He et al., 2015; Guemiza et al., 2017), is  
48 highly dependent on pH, being low at  $pH < 5.0$  ( $\leq 14$  mg/L) but very high at  $pH > 6.0$   
49 ( $> 100$  mg/L) since its anionic form is predominant. As a result, it has been detected  
50 in industrial wastewater of pH 9.0 at a concentration of 490 mg/L (Rahmani et al.,  
51 2018). Various technologies have been developed for the treatment of PCP in water,  
52 including biodegradation (Khan et al., 2017), adsorption (Zhou et al., 2014), chemical  
53 oxidation and reduction (Shih et al., 2016), electrochemical oxidation (Niu et al., 2013)  
54 and photocatalysis (Khuzwayo and Chirwa, 2017). Unfortunately, most of these  
55 methods exhibit several weaknesses like long treatment times required, high energy

56 consumption, insufficient ability to ensure total removal and inefficient mineralization  
57 that causes the accumulation of toxic intermediates.

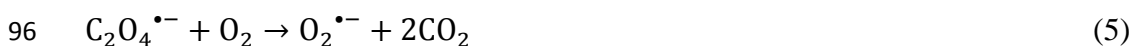
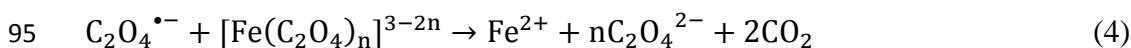
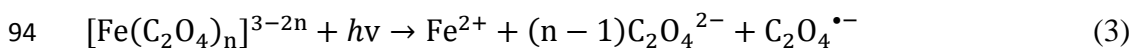
58 Nowadays, advanced oxidation processes (AOPs), including those based on  
59 Fenton's reaction, ozone and light irradiation, have been proven excellent to degrade  
60 highly recalcitrant organic compounds because of the action of hydroxyl radical  
61 ( $\cdot\text{OH}$ ), which is the second strongest oxidant after fluorine with a high standard redox  
62 potential ( $E = 2.80 \text{ V|SHE}$ ) (Martínez-Huitle et al., 2015). Among AOPs, Fenton's  
63 reaction is recognized as a very simple way to generate  $\cdot\text{OH}$ . However, inefficient  
64 Fe(II) regeneration usually results in the need of large amounts of such catalyst, which  
65 must be carefully managed upon treatment completion (Brillas et al., 2009). The  
66 addition of UV irradiation gives rise to photo-Fenton process, which can readily  
67 regenerate Fe(II) and produce additional  $\cdot\text{OH}$  amounts (Eq. (1)), as well as  
68 photodecarboxylate the Fe(III) complexes generated during the oxidation of most  
69 organics (Eq. (2)) (Ye et al., 2016).



72 Nonetheless, conventional Fenton process with simple soluble salts presents two  
73 critical limitations: (i) it demands acidic conditions (pH 2.5-3.5) to maintain a high  
74 performance, which restricts the application of photo-Fenton process for wastewater  
75 treatment at large scale; and (ii) reaction (1) exhibits a quite low quantum yield for  
76 Fe(III) photoreduction ( $\Phi(\text{Fe}(\text{II})) = 0.14 \pm 0.04$  at 313 nm), and might also be

77 inhibited by the reduced light penetration when treating colored solutions (Pignatello  
78 et al., 2006).

79 To overcome these disadvantages, some chelating agents such as oxalate, citrate,  
80 ethylenediamine-N,N'-disuccinic acid (EDDS), ethylenediaminetetraacetic acid  
81 (EDTA) and nitrilotriacetic acid (NTA) have been investigated to upgrade the  
82 conventional photo-Fenton process (Klamerth et al., 2012; Manenti et al., 2015;  
83 Clarizia et al., 2017). Such compounds are able to form stable complexes with ferric  
84 ions, thereby maintaining the iron soluble at less acidic pH and acting as photoactive  
85 species that greatly enhance the performance of photo-Fenton process. Among these  
86 agents, oxalate has been shown to be preferred (Kwan and Chu, 2007). The  
87 advantages of ferrioxalate-assisted photo-Fenton as compared to other systems  
88 include (Luca et al., 2014; Souza et al., 2014; Clarizia et al., 2017): (i) the soluble  
89 ferrioxalate complex allows working at neutral pH values; (ii) this complex has a  
90 higher quantum yield for Fe(II) regeneration (Eqs. (3,4)); (iii) it exhibits more intense  
91 light absorption, with a range up to 580 nm; and (iv) additional H<sub>2</sub>O<sub>2</sub> production can  
92 occur from participation of dissolved oxygen (Eqs. (5-8)). The reaction network was  
93 summarized as follows (Souza et al., 2014; Clarizia et al., 2017):





100 Considering the high energy consumption using artificial UV light sources,  
101 sunlight can be alternatively employed to operate the ferrioxalate-assisted solar  
102 photo-Fenton process, which has been proven to be an efficient wastewater treatment  
103 technology (Monteagudo et al., 2010; Souza et al., 2014; Expósito et al., 2018). The  
104 present work investigates the mineralization and dechlorination of PCP by  
105 ferrioxalate-assisted solar photo-Fenton process at mild pH with a low iron  
106 concentration. The effect of main experiment parameters, such as initial  
107 concentrations of  $\text{H}_2\text{O}_2$  and  $\text{Fe(II)}$ , pH and iron/oxalic acid molar ratios on total  
108 organic carbon (TOC) abatement has been assessed, and the accumulation of  $\text{H}_2\text{O}_2$ ,  
109  $\text{Fe(II)}$  and dissolved  $\text{O}_2$  has also been determined. In addition, a schematic reaction  
110 mechanism involving the iron cycle, radical reactions and PCP mineralization has  
111 been proposed. A possible pathway for the degradation of PCP is presented according  
112 to the identified intermediates.

## 113 **2. Experimental**

### 114 *2.1 Chemicals*

115 PCP was purchased from Sigma Aldrich (97% purity) and used without further  
116 purification. Hydrogen peroxide, ferrous sulfate heptahydrate and oxalic acid  
117 dihydrate were obtained from Union Chemical, Merck and Sigma Aldrich,  
118 respectively. The solution pH was adjusted with diluted NaOH or  $\text{H}_2\text{SO}_4$ . Other  
119 chemicals used herein were of analytical grade. Laboratory-grade deionized water

120 from a reverse osmosis system (resistivity > 18.2 MΩ cm) was used to prepare all  
121 aqueous solutions.

## 122 *2.2 Experimental procedures*

123 The experiments were carried out in an undivided glass cell filled with 1 L of  
124 PCP solution, under constant magnetic stirring and pH monitoring (see setup in Fig.  
125 S1). All the trials were performed with the initial PCP concentration fixed at 50 mg/L,  
126 which is almost the solubility limit of PCP at circumneutral pH. In the dark, oxalic  
127 acid was mixed with the pollutant solution and then, the Fe(II) salt was added as  
128 catalyst source. The mixture was homogenized for 5 min before pH adjustment.  
129 Finally, as the cell was exposed to sunlight, a small H<sub>2</sub>O<sub>2</sub> volume was added to  
130 initiate the photo-Fenton treatment. Samples were withdrawn at different time  
131 intervals, being immediately mixed with NaOH to quench the reaction and then  
132 analyzed after filtration on a 0.22 μm syringe filter. The pH was controlled along the  
133 experiments to keep an almost constant value. The average UVA irradiance upon  
134 exposure to sunlight was measured on a UV radiometer (SENTRY<sup>®</sup>, ST-513), placed  
135 next to the cell, which measured within the wavelength range from 290 to 370 nm. All  
136 the trials were performed between 11 am and 2 pm on sunny days from May to June  
137 2017 at Tainan (Taiwan). As can be observed in Fig. S2, during this period the  
138 average UVA irradiance was around 40 W/m<sup>2</sup>. Note that, UVA irradiance showed  
139 approximately 7.6 W/m<sup>2</sup> difference at 11 AM between May and June. Fortunately, it  
140 is believed that such difference has insignificant influence on the performance of  
141 ferrioxalate-assisted solar photo-Fenton process (Souza et al., 2014).

### 142 2.3 Analytical methods

143 The mineralization of PCP solutions was assessed from the time course of TOC,  
144 measured on a TOC analyzer (Sievers 900, GE). The residual amount of H<sub>2</sub>O<sub>2</sub> during  
145 the treatment was analyzed using the titanium sulfate method (Eisenberg, 1943). The  
146 Fe(II) concentration was measured using the 1,10-phenanthroline method (Tamura et  
147 al., 1974). Released Cl<sup>-</sup> ions were quantified by inductively coupled plasma optical  
148 emission spectrometry (Ultima 2000 ICP-OES spectrometer from Horiba Scientific).  
149 Dissolved oxygen (DO) was measured on an Oxi 3210 instrument from WTW. The  
150 carboxylic acids were determined at  $\lambda = 210$  nm by ion-exclusion HPLC using a  
151 Waters 600 LC fitted with a Bio-Rad Aminex HPX 87H, 300 mm  $\times$  7.8 mm, column  
152 at 35 °C. The elution was carried out by using 4 mM H<sub>2</sub>SO<sub>4</sub> as mobile phase at 0.6  
153 mL/min. The aromatic by-products were analyzed by gas chromatography coupled to  
154 mass spectrometry (GC-MS) using an Agilent Technologies system composed of a  
155 6890N gas chromatograph and a 5975C mass spectrometer operating in EI mode at 70  
156 eV. Around 150 mL of aqueous sample was withdrawn from the cell to extract the  
157 organic components with CH<sub>2</sub>Cl<sub>2</sub> in three times (25 mL each). The resulting organic  
158 solution was dried over anhydrous Na<sub>2</sub>SO<sub>4</sub>, filtered and concentrated to less than 1  
159 mL under reduced pressure to be further analyzed. The mass spectra were identified  
160 with support from NIST05 MS library.

## 161 3. Results and discussion

### 162 3.1. Comparative study of PCP mineralization



163 First, a comparative study on the mineralization of PCP from an aqueous solution  
164 containing 50 mg/L (i.e., 14 mg/L TOC) at pH 5.0 by different processes was  
165 conducted. As shown in Fig. 1, direct solar photolysis had no effect on TOC  
166 abatement for 120 min. This agrees with the low photodegradation rate constants at  
167 PCP concentrations of 0.4-2.1 mg/L, within the range of  $4.9 \times 10^{-2}$ - $7.1 \times 10^{-2}$  h<sup>-1</sup>, which  
168 informs about the great persistence of this pollutant in the environment (Agbo et al.,  
169 2011). The PCP mineralization by conventional Fenton process with 2 mM H<sub>2</sub>O<sub>2</sub> was  
170 also very inefficient due to the low Fe(II) dosage (i.e., 5 mg/L) and the expected  
171 Fe(III) precipitation at pH 5.0. When the same trial was carried out in the presence of  
172 1.2 mM oxalic acid, a negligible enhancement of mineralization was achieved. Under  
173 such conditions, in spite of the solubilization of Fe(III) upon chelation with oxalate,  
174 the regeneration of Fe(II) to promote Fenton's reaction was quite poor. A much better  
175 performance was shown by processes with sunlight irradiation. Solar photo-Fenton  
176 process with 5 mg/L Fe(II) and 2 mM H<sub>2</sub>O<sub>2</sub> yielded 21% TOC decay after 120 min.  
177 Such an upgrade as compared to trials in the dark can be mainly explained by the  
178 photoreduction of Fe(III)-hydroxy complexes to generate Fe(II) and <sup>•</sup>OH (Eq. (1)),  
179 along with the photodecarboxylation of Fe(III) complexes of by-products formed  
180 during the degradation of PCP (Eq. (2)). TOC abatement increased up to 50% in  
181 ferrioxalate-assisted solar photolysis process with 1.2 mM H<sub>2</sub>C<sub>2</sub>O<sub>4</sub>. According to Eqs.  
182 (3)-(8), O<sub>2</sub><sup>•-</sup> and <sup>•</sup>OH can be generated via several chain reactions in the presence of  
183 O<sub>2</sub> and hence, these two radical species may play key roles for the degradation of the  
184 parent molecule and its by-products. However, the limited dissolved oxygen

185 concentration in the solution significantly restricted the importance of Eqs. (5) and  
186 (6), which allows explaining the slower PCP removal from 30 min. The most  
187 effective process to degrade PCP was ferrioxalate-assisted solar photo-Fenton,  
188 yielding 97.5% TOC removal at 120 min, accompanied by the precipitation of iron  
189 hydroxide. Note that, although the addition of 1.2 mM  $\text{H}_2\text{C}_2\text{O}_4$  accounted for 28.8  
190 mg/L TOC, almost total abatement organic carbon from PCP and oxalic acid was  
191 attained in the ferrioxalate-assisted solar photo-Fenton process. This positive result is  
192 attributed to the high yield of  $\cdot\text{OH}$  formed in the presence of sufficient  $\text{H}_2\text{O}_2$  and  
193 efficiently regenerated Fe(II) by Eqs. (3) and (4).

### 194 *3.2. Effect of $\text{H}_2\text{O}_2$ and Fe(II) dosage*

195 The amount of added  $\text{H}_2\text{O}_2$  plays a relevant role in ferrioxalate-assisted solar  
196 photo-Fenton process, as it is the source of  $\cdot\text{OH}$  upon catalyzed decomposition with  
197 Fe(II). Several trials were carried out with solutions of 50 mg/L PCP with 5 mg/L  
198 Fe(II) and 1.2 mM  $\text{H}_2\text{C}_2\text{O}_4$  at pH 5.0, employing different  $\text{H}_2\text{O}_2$  concentrations. As  
199 shown in Fig. 2a, the decay of TOC after 120 min of irradiation increased from 50%  
200 to 97% when the  $\text{H}_2\text{O}_2$  content was increased from 0 to 1.5 mM. Further increase of  
201  $\text{H}_2\text{O}_2$  dosage up to 2.5 mM resulted in a quicker mineralization during the first 60  
202 min, whereupon close profiles were observed until reaching the same TOC removals  
203 at the end of the treatments. The significant acceleration using up to 1.5 mM  $\text{H}_2\text{O}_2$   
204 was then due to the faster production of  $\cdot\text{OH}$  from Fenton's reaction (Soares et al.,  
205 2015). However, an excess of  $\text{H}_2\text{O}_2$  was detrimental because: (i) it acts as a radical  
206 scavenger, greatly reducing the amount of  $\cdot\text{OH}$  according to Eqs. (9) and (10), and (ii)

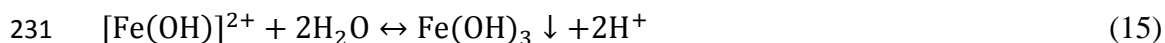
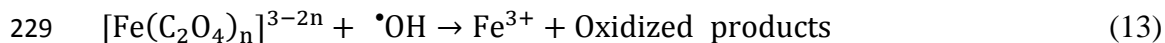
207 it accelerates its self-decomposition from Eq. (11) (Vedrenne et al., 2012; Pouran et  
208 al., 2015).



212 In order to elucidate the effect of Fe(II) dosage on the mineralization ability of  
213 the ferrioxalate-assisted solar photo-Fenton treatment of solutions of 50 mg/L PCP,  
214 Fe(II) catalysts amounts within the range of 2-10 mg/L were added in the presence of  
215 2.0 mM H<sub>2</sub>O<sub>2</sub> and 1.2 mM H<sub>2</sub>C<sub>2</sub>O<sub>4</sub> at pH 5.0. The results depicted in Fig. 2b illustrate  
216 a significant enhancement of TOC abatement upon increase of Fe(II) dosage within  
217 the early stage (~ 20 min). Hence, a higher catalyst concentration greatly accelerated  
218 the decomposition of H<sub>2</sub>O<sub>2</sub>, which resulted in a larger accumulation of  $\cdot\text{OH}$   
219 responsible for the mineralization. However, the final TOC removal at 120 min  
220 decreased from 97.5% to 91.4% when the dosage was increased from 5 mg/L to 10  
221 mg/L. On the one hand, an excessive addition of Fe(II) promotes partial radical  
222 scavenging according to Eq. (12) (Monteagudo et al., 2010).



224 Furthermore, rapid accumulation of  $\cdot\text{OH}$  during the initial stage is associated to a  
225 quicker decomposition of oxalate ligand and iron/oxalate complex (Eq. (13)). As the  
226 treatment proceeds, an increasing amount of Fe(III) cannot be complexed and  
227 maintained soluble and stable, which stimulates the formation of [Fe(OH)]<sup>2+</sup> (Eq. (14))  
228 and its further hydrolysis and precipitation as Fe(OH)<sub>3</sub> (Eq. (15)) (Pliego et al., 2014).



232 In addition, a larger quantity of Fe(III) hydroxyde sludge may reduce the  
233 transparency of the solution, thus reducing the photocatalysis efficiency.

### 234 3.3. Effect of pH and iron/oxalic acid ratio

235 Since PCP is quite insoluble at low pH, supersaturated PCP solutions (i.e., 50  
236 mg/L) were prepared to start the experiments at pH 5.0. After 15 min of  
237 ferrioxalate-assisted solar photo-Fenton treatment, the pH was adjusted to a given  
238 value to investigate its effect on TOC decay. As can be seen in Fig. 2c, similar trends  
239 reaching more than 95% TOC removal at 120 min were obtained at  $\text{pH} \leq 6.0$  in the  
240 presence of 5 mg/L Fe(II), 2 mM  $\text{H}_2\text{O}_2$  and 1.2 mM  $\text{H}_2\text{C}_2\text{O}_4$ , which demonstrates the  
241 feasibility of working at mild pH thanks to the use of ferrioxalate complexes. In  
242 contrast, at  $\text{pH} \geq 7$ , TOC remained almost constant, probably as a result of massive  
243 iron precipitation. Indeed, pH plays a crucial role regarding the speciation of iron,  
244 oxalic acid and ferrioxalate complexes (Panias et al., 1996). Different species  
245 including  $\text{H}_2\text{C}_2\text{O}_4$ ,  $\text{HC}_2\text{O}_4^-$  and  $\text{C}_2\text{O}_4^{2-}$  may coexist in aqueous medium, since oxalic  
246 acid exhibits two ionization equilibria ( $\text{p}K_1 = 1.25$  and  $\text{p}K_2 = 4.27$ ).  $\text{C}_2\text{O}_4^{2-}$ , the  
247 predominant species at  $\text{pH} > 4.27$ , is considered as the main source to form different  
248 ferrioxalate complexes in the presence of iron, being the complex formed by  $\text{HC}_2\text{O}_4^-$   
249 negligible at  $\text{pH} > 2.0$  (Souza et al., 2014). The performance of ferrioxalate-assisted  
250 solar photo-Fenton process highly depends on the photoactivity and stability of iron

251 complexes, whose species distribution depends on both, solution pH and iron/oxalic  
252 acid ratio. Fig. S3 reveals the Fe(III) speciation diagrams as a function of pH in the  
253 presence of 5 mg/L Fe(II) with different iron/oxalic acid molar ratios, as determined  
254 using MATLAB. The corresponding equilibrium reactions and constants are listed in  
255 Table S1. As can be seen in Fig S3 (e), which shows the speciation corresponding to  
256 the case in which the same Fe(II) and oxalic acid concentrations of trials of Fig. 2c are  
257 used, the predominant species are  $\text{Fe}(\text{C}_2\text{O}_4)_3^{3-}$  and  $\text{Fe}(\text{C}_2\text{O}_4)_2^-$  at  $3.0 < \text{pH} < 7.0$ . The  
258 former ferrioxalate complex is considered as the most stable and photoactive iron  
259 complex (Faust and Zepp, 1993), being efficiently photoreduced to Fe(II) that reacts  
260 with  $\text{H}_2\text{O}_2$  to generate  $\cdot\text{OH}$ . This is highly consistent with the profiles presented in  
261 Fig. 2c, evidencing an outstanding performance and negligible difference of TOC  
262 decays when pH varied from 3.0 to 6.0. Conversely, only 3.7% mineralization was  
263 achieved once the pH of the PCP solution was adjusted to 7.0, which can be  
264 accounted for by: (i) the preferential precipitation of Fe(III) over ferrioxalate  
265 formation (Fig. S3e), (ii) the gradual photodecarboxylation of ferrioxalate complexes,  
266 which accelerates the formation of  $\text{Fe}(\text{OH})_{3(\text{s})}$ , and (iii) the enhanced transformation  
267 of  $\cdot\text{OH}$  into  $\text{O}_2^{\cdot-}$  at high pH.

268 Several experiments were performed at pH 5.0 to evaluate the effect of the  
269 iron/oxalic acid ratio. As shown in Fig. 2d, almost complete TOC removal was  
270 obtained at molar ratios of 1:6, 1:10 and 1:13.5, whereas only 21.4% mineralization  
271 was achieved without the addition of oxalic acid. In the absence of oxalate anion, the  
272 predominant Fe(III) species at pH 5.0 is  $[\text{Fe}(\text{OH})_2]^+$  (Fig. S3a), which is much less

273 photoactive than  $[\text{Fe}(\text{OH})]^{2+}$  that is typically formed in conventional Fenton process  
274 at pH  $\sim$  3.0 (Eq. (1)). Using the 1:3 iron/oxalic acid ratio,  $\text{Fe}(\text{C}_2\text{O}_4)_3^{3-}$  (56.0%) and  
275  $\text{Fe}(\text{C}_2\text{O}_4)_2^-$  (43.1%) account for the largest proportion of Fe(III) species at pH 5.0  
276 (Fig. S3b). The higher photoactivity of these complexes enhances the regeneration of  
277 Fe(II), yielding a greater mineralization as compared to the trial with 1:0 ratio (Fig.  
278 2d). Increasing the iron/oxalic acid ratio to 1:6 (Fig. S3c), the molar fraction of the  
279 very photoactive  $\text{Fe}(\text{C}_2\text{O}_4)_3^{3-}$  complex increases to 89.9% , with  $\text{Fe}(\text{C}_2\text{O}_4)_2^-$   
280 decreasing to 10.1% at pH 5.0, which justifies the faster and almost complete TOC  
281 decay. The abatement was slightly decelerated at ratios of 1:10 and 1:13.5 (Fig. 2d),  
282 despite the fact that the  $\text{Fe}(\text{C}_2\text{O}_4)_3^{3-}$  species accounted for more than 95% of Fe(III),  
283 because of the significant increase of initial TOC in solution from oxalic acid that  
284 competed with PCP to react with  $\cdot\text{OH}$ .

285 It can then be concluded that the optimum performance of the  
286 ferrioxalate-assisted solar photo-Fenton process takes place at pH 5.0, with an  
287 iron/oxalic acid molar ratio of 1:6.

#### 288 *3.4. Evolution of $\text{H}_2\text{O}_2$ , Fe(II) and dissolved $\text{O}_2$*

289 The evolution of  $\text{H}_2\text{O}_2$  and Fe(II) along the ferrioxalate-assisted solar  
290 photo-Fenton treatments collected in Fig. 2d is depicted in Fig. 3a and b, respectively.  
291 As shown in Fig. 3a, 40% consumption of  $\text{H}_2\text{O}_2$  was achieved after 120 min in the  
292 absence of oxalic acid, whereas it reached more than 93% in only 60 min at all  
293 iron/oxalic acid ratios, thus confirming the efficient Fe(II) regeneration upon  
294 photoreduction of the ferrioxalate complexes. More in detail, rising the molar ratio

295 from 1:3 to 1:6 accelerated the decomposition of  $\text{H}_2\text{O}_2$ , but further increase of oxalic  
296 acid content slowed down the  $\text{H}_2\text{O}_2$  disappearance. In fact, the  $\text{H}_2\text{O}_2$  concentration  
297 measured at 2 and 5 min using a molar ratio of 1:13.5 was even higher than that at  
298 time zero, which can be attributed to the additional generation of  $\text{H}_2\text{O}_2$  from the  
299 reaction sequence given by Eqs. (3)-(8). As can be observed, DO plays a major role in  
300 the formation of  $\text{H}_2\text{O}_2$  and hence, its evolution with treatment time was evaluated in  
301 different cases. As depicted in Fig.4, the concentration of oxygen dissolved in the  
302 PCP solution decreased considerably in ferrioxalate-assisted solar photo-Fenton and  
303 solar photolysis processes, whereas it remained stable in conventional Fenton and  
304 solar photo-Fenton, which verifies the key role of DO in the aforementioned reactions  
305 to form  $\text{H}_2\text{O}_2$ . This means that this additional amount of  $\text{H}_2\text{O}_2$  is able to react with  
306 Fe(II) to generate  $\cdot\text{OH}$ , which combined with other radical species ( $\text{C}_2\text{O}_4^{\cdot-}$ ,  $\text{CO}_2^{\cdot-}$  and  
307  $\text{O}_2^{\cdot-}$ ) is responsible for the greater TOC abatement in ferrioxalate-assisted solar  
308 processes (Fig. 1). Note that the DO concentration in both ferrioxalate systems tended  
309 to increased again from 30 min, which can be explained by the quick chemical and  
310 photochemical decomposition of ferrioxalate complexes, especially in solar  
311 photo-Fenton process (Fig. 1).

312 On the other hand, Fig. 3b reveals the evolution of Fe(II) at different iron/oxalic  
313 acid ratios. The catalyst concentration decreased to less than 1 mg/L in only 2 min in  
314 the absence of oxalate because of the quick consumption by  $\text{H}_2\text{O}_2$ . The resulting  
315 Fe(III) ion was pre-eminently in a poorly photoactive form at pH 5.0 ( $[\text{Fe}(\text{OH})_2]^+$ , see  
316 Fig. S3a), thus being difficult to regenerate Fe(II). The decrease in Fe(II)

317 concentration was greatly decelerated upon increase of oxalic acid content, which  
318 confirms the very efficient photoreduction of ferrioxalate complexes. Nevertheless,  
319 owing to oxalic acid decomposition, the generated Fe(III) tended to precipitate at pH  
320 5.0, eventually causing the decrease of Fe(II) concentration. Theoretically, all iron  
321 should be complexed at iron/oxalic acid molar ratios higher than 1:3 (Souza et al.,  
322 2014), but the continuous photodecarboxylation and decomposition of ferrioxalate  
323 complexes by  $\cdot\text{OH}$  could cause the partial precipitation of iron. However, the use of a  
324 large amount of oxalic acid ensures the ion stabilization by formation of ferrioxalate  
325 complexes, especially at pH higher than 3.1. As can be seen in Fig. 3b, the  
326 concentration of Fe(II) kept the highest value (i.e., 5 mg/L) for 20 min at an  
327 iron/oxalic acid molar ratio of 1:13.5, which is very positive to promote Fenton's  
328 reaction. Nonetheless, an excessively high amount of oxalic acid increases the  
329 operation costs, causes the competition with PCP to react with  $\cdot\text{OH}$  and results in a  
330 higher initial TOC and thus, the iron/oxalic acid ratio should be carefully considered  
331 for real applications.

### 332 *3.5. Possible reaction mechanism of ferrioxalate-assisted solar photo-Fenton process*

333 Based on all previous results, a reaction mechanism for the ferrioxalate-assisted  
334 solar photo-Fenton treatment of PCP is proposed in Fig. 5.  $\text{Fe}^{3+}$  can be complexed by  
335 oxalate, and the efficient photoreduction of the resulting Fe(III) complexes eventually  
336 yields Fe(II), either as free  $\text{Fe}^{2+}$  or complexed with oxalate, which readily reacts with  
337  $\text{H}_2\text{O}_2$  to generate  $\cdot\text{OH}$  and Fe(III) in a closed loop. However, owing to the progressive  
338 decomposition of ferrioxalate complexes, the excess of Fe(III) tends to precipitate as



339  $\text{Fe}(\text{OH})_{3(s)}$  at pH higher than 3.1. In the presence of  $\text{O}_2$ , additional amounts of  $\text{H}_2\text{O}_2$   
340 and concomitant radical species ( $\text{C}_2\text{O}_4^{\cdot-}$ ,  $\text{CO}_2^{\cdot-}$ ,  $\text{HO}_2^{\cdot}$  and  $\text{O}_2^{\cdot-}$ ) can be generated  
341 according to a series of radical reactions, although their oxidization ability is much  
342 weaker than that of  $\cdot\text{OH}$ . Therefore, the degradation and mineralization of PCP can be  
343 pre-eminently explained in terms of reactions with  $\cdot\text{OH}$ , as in the case of classical  
344 Fenton's reaction.

### 345 *3.6. Identification of degradation by-products*

346 In surface water and sediments, the toxicity of PCP has been evidenced at  
347 concentrations greater than 3 mg/L (Stepanova et al., 2000). Some intermediates  
348 generated during the degradation of this target pollutant, like 3,4,5-trichlorophenol,  
349 are known to be even more toxic, as the toxicity is related to the number of chlorine  
350 atoms and their position (Lin et al., 2018). Therefore, the release of  $\text{Cl}^-$  and the  
351 generation of PCP reaction by-products have been investigated. Fig. 6a reveals the  
352 evolution of  $\text{Cl}^-$  ion with irradiation time during the ferrioxalate-assisted solar  
353 photo-Fenton treatment of 50 mg/L PCP with 5 mg/L Fe(II), 2 mM  $\text{H}_2\text{O}_2$  and 1.2 mM  
354  $\text{H}_2\text{C}_2\text{O}_4$ . As can be seen, the degradation of PCP was accompanied by a continuous  
355 release of  $\text{Cl}^-$ , whose concentration increased with over time up to attain 33.5 mg/L  
356 (i.e., 100% release) at 90 min, thus informing about the excellent dechlorination  
357 performance and the total removal of organochlorine intermediates generated during  
358 the degradation of PCP in this process. Fig. 6b reveals the evolution of five carboxylic  
359 acids like oxalacetic, malonic, succinic, formic and acetic resulting from the cleavage  
360 of the aromatic rings. The maximum concentration of succinic acid was 5.9 mg/L at

361 30 min, whereas lower contents of the other acids were accumulated, reaching  
362 maximum values of 2.1, 1.4, 0.9 and 0.7 mg/L for malonic, oxalacetic, formic and  
363 acetic acids at 20, 30, 45 and 45 min, respectively. The accumulation of these  
364 carboxylic acids entails the occurrence of competing Fe(III)-carboxylate complexes,  
365 which efficiently enhanced the Fe(II) regeneration via Eq. (2). Moreover, all the acids  
366 disappeared in 90-120 min, confirming the almost total mineralization achieved by  
367 ferrioxalate-assisted solar photo-Fenton process.

368 The main transformation products (TPs) identified by GC-MS analysis included  
369 four monobenzenic and four polycyclic molecules. As summarized in Table S2, these  
370 corresponded to tetrachlorophenol (TeCP), trichlorophenol (TriCP),  
371 trichlorohydroquinone (TrCHQ), tetrachlorohydroquinone (TeCHQ),  
372 hexachlorodibenzofuran (HCDF), pentachlorodibenzo-*p*-dioxin (PCDD),  
373 hexachlorodibenzo-*p*-dioxin (HCDD) and octachlorodibenzo-*p*-dioxin (OCDD). The  
374 cleavage of C-Cl bonds yielded lower chlorinated structures like TeCP and TriCP  
375 (Liu et al., 2004). The subsequent attack of  $\cdot\text{OH}$  onto their aromatic rings resulted in  
376 two hydroxylated TPs (TeCHQ and TrCHQ). Alternatively, the direct attack of  $\cdot\text{OH}$   
377 on C-Cl bonds of PCP can give rise to TeCHQ, which may be further dechlorinated.  
378 On the other hand, several dimeric structures were identified. Since PCP mainly exists  
379 as anionic form ( $\text{PCP}^-$ ) at  $\text{pH} > 4.7$ , hydroxylation of  $\text{PCP}^-$  leads to the generation of  
380 pentachlorophenoxy radical ( $\text{PCP}^\bullet$ ). Then, the coupling reaction between two  $\text{PCP}^\bullet$   
381 species or  $\text{PCP}^\bullet$  and  $\text{PCP}^-$  may yield OCDD and HCDF, respectively, with chloride  
382 release (Fukushima and Tatsumi, 2001). Further dechlorination of OCDD caused the

383 formation of lower chlorinated derivatives like HCDD and PCDD. The degradation  
384 routes of PCP, which are depicted in Fig. 7, on the basis of the identified by-products,  
385 involve three paths: dechlorination, hydroxylation and dimerization.

#### 386 **4. Conclusions**

387 Promising results were obtained for the mineralization of PCP at near-neutral pH  
388 using a low iron concentration by the ferrioxalate-assisted solar photo-Fenton process.  
389 More than 95% TOC abatement were achieved in 120 min. The optimized operation  
390 parameters were: 5 mg/L Fe(II), 1.5 mM H<sub>2</sub>O<sub>2</sub>, pH 5.0 and iron/oxalic acid molar  
391 ratio of 1:6. The presence of oxalic acid greatly enhances the performance of solar  
392 photo-Fenton process due to various reasons: (i) the ferrioxalate complex ensures the  
393 iron solubility at mild pH; (ii) the Fe(III) complexes with oxalate are highly  
394 photoactive, thus allowing the continuous Fe(II) regeneration; and (iii) additional  
395 amounts of H<sub>2</sub>O<sub>2</sub> and radical species are generated with the involvement of O<sub>2</sub>. It was  
396 shown that pH and iron/oxalic acid molar ratio play crucial roles on the Fe(III)  
397 speciation in aqueous medium, greatly influencing the performance of the degradation  
398 process. At pH 3.0-7.0 and iron/oxalic acid ratio higher than 1:3, all the iron is  
399 complexed with oxalate, whereas the excess of oxalate ion remains in solution and  
400 ensures the continuous formation of ferrioxalate complexes that impedes the iron  
401 precipitation. The mineralization of PCP involves dechlorination, hydroxylation and

402 decarboxylation steps, as well as the formation of some dimers that can be gradually  
403 degraded by  $\cdot\text{OH}$  and other radicals.

#### 404 **Acknowledgements**

405 This work was supported by Natural Science Foundation of Hubei Province,  
406 China (Grant 2012FFA089) and the National Science Council of the Republic of  
407 China (No. NSC 102-2622-E-006-004-CC2). The authors also thank financial support  
408 from project CTQ2016-78616-R (AEI/FEDER, EU) and PhD scholarship awarded to  
409 Z.H. Ye (State Scholarship Fund, CSC, China).

#### 410 **References**

- 411 Agbo. S.O., Küster, E., Georgi, A., Akkanen, J., Leppänen, M.T., Kukkonen, J.V.K.,  
412 2011. Photostability and toxicity of pentachlorophenol and phenanthrene. J.  
413 Hazard. Mater. 189, 235-240.
- 414 Amendola, L., Cortese, M., Vinatoru, D., Sposato, S., Insogna, S., 2017. Innovative  
415 analytical method for the determination of underivatized tributyltin and  
416 pentachlorophenol in seawater by gas chromatography-triple quadrupole mass  
417 spectrometry. Anal. Chim. Acta 975, 70-77.
- 418 Brillas, E., Sirés, I., Oturan, M.A., 2009. Electro-Fenton process and related  
419 electrochemical technologies based on Fenton's reaction chemistry. Chem. Rev.  
420 109, 6570-6631.
- 421 Clarizia, L., Russo, D., Somma, I.D., Marotta, R., Andreozzi, R., 2017. Homogeneous  
422 photo-Fenton processes at near neutral pH: A review. Appl. Catal. B: Environ.

423 209, 358-371.

424 Cui, Y., Liang, L., Zhong, Q., He, Q., Shan, X., Chen, K., Huang, F., 2017. The  
425 association of cancer risks with pentachlorophenol exposure: Focusing on  
426 community population in the areas along certain section of Yangtze River in  
427 China, *Environ. Pollut.* 224, 729-738.

428 Eisenberg, G.M., 1943. Colorimetric determination of hydrogen peroxide. *Ind. Eng.*  
429 *Chem. Anal. Ed.* 15, 327-328.

430 Expósito, A.J., Monteagudo, J.M., Durán, A., Martín, I.S., González, L., 2018. Study  
431 of the intensification of solar photo-Fenton degradation of carbamazepine with  
432 ferrioxalate complexes and ultrasound. *J. Hazard. Mater.* 342, 597-605.

433 Faust, B.C., Zepp, R.G., 1993. Photochemistry of aqueous iron(III)-polycarboxylate  
434 complexes: roles in the chemistry of atmospheric and surface waters. *Environ.*  
435 *Sci. Technol.* 27, 2517-2522.

436 Fukushima, M., Tatsumi, K., 2001. Degradation pathways of pentachlorophenol by  
437 photo-Fenton systems in the presence of iron(III), humic acid, and hydrogen  
438 peroxide. *Environ. Sci. Technol.* 35, 1771-1778.

439 Guemiza, K., Coudert, L., Metahni, S., Mercier, G., Besner, S., Blais, J.F., 2017.  
440 Treatment technologies used for the removal of As, Cr, Cu, PCP and/or PCDD/F  
441 from contaminated soil: A review. *J. Hazard. Mater.* 333, 194-214.

442 He, Y., Zeng, F., Lian, Z., Xu, J., Brookes, P.C., 2015. Natural soil mineral  
443 nanoparticles are novel sorbents for pentachlorophenol and phenanthrene  
444 removal. *Environ. Pollut.* 205, 43-51.

445 Hechmi, N., Bosso, L., El-Bassi, L., Scelza, R., Testa, A., Jedidi, N., Rao, M.A., 2016.  
446 Depletion of pentachlorophenol in soil microcosms with *Byssochlamys nivea*  
447 and *Scopulariopsis brumptii* as detoxification agents. *Chemosphere* 165,  
448 547-554.

449 Khan, M.D., Khan, N., Nizami, A.S., Rehan, M., Sabir, S., Khan, M.Z., 2017. Effect  
450 of co-substrates on biogas production and anaerobic decomposition of  
451 pentachlorophenol. *Bioresour. Technol.* 238, 492-501.

452 Khuzwayo, Z., Chirwa, E.M.N., 2017. The impact of alkali metal halide electron  
453 donor complexes in the photocatalytic degradation of pentachlorophenol. *J.*  
454 *Hazard. Mater.* 321, 424-431.

455 Klamerth, N., Malato, S., Agüera, A., Fernández-Alba, A., Mailhot, G., 2012.  
456 Treatment of municipal wastewater treatment plant effluents with modified  
457 photo-Fenton as a tertiary treatment for the degradation of micro pollutants and  
458 disinfection. *Environ. Sci. Technol.* 46, 2885-2892.

459 Kwan, C.Y., Chu, W., 2007. The role of organic ligands in ferrous-induced  
460 photochemical degradation of 2,4-dichlorophenoxyacetic acid. *Chemosphere* 67,  
461 1601–1611.

462 Lin, J., Meng, J., He, Y., Xu, J., Chen, Z., Brookes, P.C., 2018. The effects of different  
463 types of crop straw on the transformation of pentachlorophenol in flooded  
464 paddy soil. *Environ. Pollut.* 233, 745-754.

465 Liu, X., Quan, X., Bo, L., Chen, S., Zhao, Y., 2004. Simultaneous pentachlorophenol  
466 decomposition and granular activated carbon regeneration assisted by

467 microwave irradiation. *Carbon* 42, 415-422.

468 Luca, A.D., Dantas, R.F., Esplugas, S., 2014. Assessment of iron chelates efficiency  
469 for photo-Fenton at neutral pH. *Water Res.* 61, 232-242.

470 Manenti, D.R., Soares, P.A., Módenes, A.N., Espinoza-Quiñones, F.R., Boaventura,  
471 R.A.R., Bergamasco, R., Vilar, V.J.P., 2015. Insights into solar photo-Fenton  
472 process using iron(III)-organic ligand complexes applied to real textile  
473 wastewater treatment. *Chem. Eng. J.* 266, 203-212.

474 Martínez-Huitle, C.A., Rodrigo, M.A., Sirés, I., Scialdone, O., 2015. Single and  
475 coupled electrochemical processes and reactors for the abatement of organic  
476 water pollutants: A critical review. *Chem. Rev.* 115, 13362-13407.

477 Monteagudo, J.M., Durán, A., Martín, I.S., Aguirre, M., 2010. Catalytic degradation  
478 of Orange II in a ferrioxalate-assisted photo-Fenton process using a combined  
479 UV-A/C-solar pilot-plant system. *Appl. Catal. B: Environ.* 95, 120-129.

480 Monteagudo, J.M., Durán, A., Aguirre, M., Martín, I.S., 2010. Photodegradation of  
481 Reactive Blue 4 solutions under ferrioxalate-assisted UV/solar photo-Fenton  
482 system with continuous addition of H<sub>2</sub>O<sub>2</sub> and air injection. *Chem. Eng. J.* 162,  
483 702-709.

484 Monteagudo, J.M., Durán, A., Aguirre, M., Martín, I.S., 2011. Optimization of the  
485 mineralization of a mixture of phenolic pollutants under a ferrioxalate-induced  
486 solar photo-Fenton process. *J. Hazard. Mater.* 185, 131-139.

487 Niu, J., Bao, Y., Li, Y., Chai, Z., 2013. Electrochemical mineralization of  
488 pentachlorophenol (PCP) by Ti/SnO<sub>2</sub>-Sb electrodes. *Chemosphere* 92,

489 1571-1577.

490 Panias, D., Taxiarchou, M., Douni, I., Paspaliaris, I., Kontopoulos, A., 1996.

491 Thermodynamic analysis of the reactions of iron oxides: dissolution in oxalic

492 acid. *Can. Metall. Q.* 35, 363-373.

493 Pignatello, J., Oliveros, E., MacKay, A., 2006. Advanced oxidation process for

494 organic contaminant destruction based on the Fenton reaction and related

495 chemistry. *Crit. Rev. Environ. Sci. Technol.* 36, 1-84.

496 Pliego, G., Zazo, J.A., Casas, J.A., Rodriguez, J.J., 2014. Fate of iron oxalates in

497 aqueous solution: The role of temperature, iron species and dissolved oxygen. *J.*

498 *Environ. Chem. Eng.* 2, 2336-2241.

499 Pouran, S.R., Aziz, A.R.A., Daud, W.M.A.W., 2015. Review on the main advances in

500 photo-Fenton oxidation system for recalcitrant wastewaters. *J. Ind. Eng. Chem.*

501 21, 53-69.

502 Rahmani A.R., Jorfi S., Asgari G., Zamani F., Almasi H, Masoumi Z., 2018. A

503 comparative study on the removal of pentachlorophenol using

504 copper-impregnated pumice and zeolite. *J. Environ. Chem. Eng.* 6, 3342-3348.

505 Shih, Y.H., Chen, M.Y., Su, Y.F., Tso, C.P., 2016. Concurrent oxidation and reduction

506 of pentachlorophenol by bimetallic zerovalent Pd/Fe nanoparticles in an oxic

507 water. *J. Hazard. Mater.* 301, 416-423.

508 Soares, P.A., Batalha, M., Souza, S.M.A.G.U., Boaventura, R.A.R., Vilar, V.J.P., 2015.

509 Enhancement of a solar photo-Fenton reaction with ferric-organic ligands for

510 the treatment of acrylic-textile dyeing. *J. Environ. Manage.* 152, 120-131.



511 Souza, B.M., Dezotti, M.W.C., Boaventura, R.A.R., Vilar, V.J.P., 2014. Intensification  
512 of a solar photo-Fenton reaction at near neutral pH with ferrioxalate complexes:  
513 A case study on diclofenac removal from aqueous solutions. *Chem. Eng. J.* 256,  
514 448-457.

515 Stepanova, L.I., Lindström-Seppä, P., Hänninen, O.O.P., Kotelevtsev, S.V., Glaser,  
516 V.M., Novikov, C.N., Beim, A.M., 2000. Lake Baikal: biomonitoring of pulp  
517 and paper mill waste water. *Aquat. Ecosyst. Health Manage.* 3, 259-269.

518 Tamura, H., Goto, K., Yotsuyanagi, T., Nagayama, M., 1974. Spectrophotometric  
519 determination of iron(III) with 1,10-phenanthroline in the presence of large  
520 amounts of iron(III). *Talanta* 21, 314-318.

521 Tsoufis, T., Katsaros, F., Kooi, B.J., Bletsas, E., Papageorgiou, S., Deligiannakis, Y.,  
522 Panagiotopoulos, I., 2017. Halloysite nanotube-magnetic iron oxide  
523 nanoparticle hybrids for the rapid catalytic decomposition of pentachlorophenol.  
524 *Chem. Eng. J.* 313, 466-474.

525 Vedrenne, M., Vasquez-Medrano, R., Prato-Garcia, D., Frontana-Uribe, B.A.,  
526 Hernandez-Esparza, M., Andrés, J.M.D., 2012. A ferrous oxalate mediated  
527 photo-Fenton system: toward an increased biodegradability of indigo dyed  
528 wastewaters. *J. Hazard. Mater.* 243, 292-301.

529 Ye, Z., Zhang, H., Yang, L., Wu, L., Qian, Y., Geng, J., Chen, M., 2016. Effect of a  
530 solar Fered-Fenton system using a recirculation reactor on biologically treated  
531 landfill leachate. *J. Hazard. Mater.* 319, 51-60.

532 Zhou, L., Pan, S., Chen, X., Zhao, Y., Zou, B., Jin, M., 2014. Kinetics and

533 thermodynamics studies of pentachlorophenol adsorption on covalently  
534 functionalized  $\text{Fe}_3\text{O}_4@\text{SiO}_2$ -MWCNTs core-shell magnetic microspheres.  
535 Chem. Eng. J. 257, 10-19.